AD-A177 468 EXPERIMENTAL VERIFICATION OF A MICROBUCKLING MODEL FOR THE AXIAL COMPRESS (U) MASSACHUSETTS UNIV AMHERST DEPT OF POLYMER SCIENCE AND ENGINE... S J DETERESA ET AL. 1/1

UNCLASSIFIED 05 JAN 87 TR-29 N00014-83-K-0228 F/G 11/3 NL

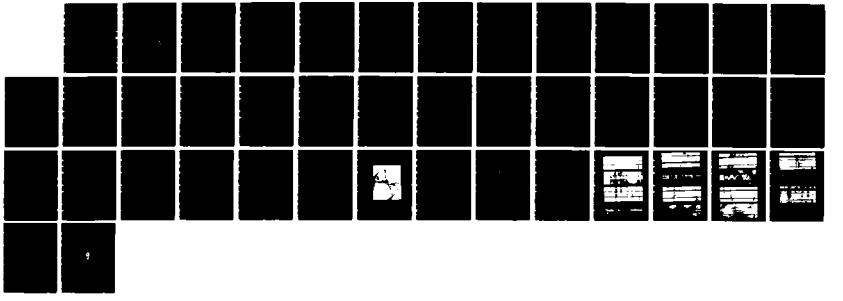

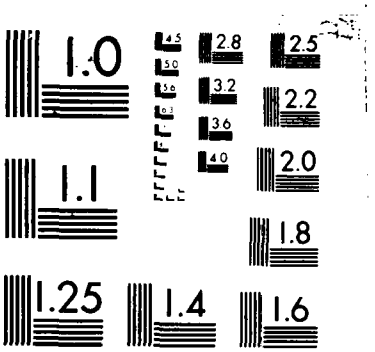

SECURITY CLASSIFICATION OF THIS PAGE (When Data Entered)

AD-A177 468

1. REPORT NUMBER: Technical Report No. 29	2. GOVT ACCESSION NO. / 3. RECIPIENT'S CATALOG NUMBER
4. TITLE (and Subtitle): Experimental Verification Of A Microbuckling Model For The Axial Compressive Failure Of High Performance Polymer Fibers	5. TYPE OF REPORT & PERIOD COVERED: Interim 6. PERFORMING ORG. REPORT NUMBER
7. AUTHOR(s): Steven J. DeTeresa, Roger S. Porter and Richard J. Farris	8. CONTRACT OR GRANT NUMBER(s): N00014-83-K-0228
9. PERFORMING ORGANIZATION NAME AND ADDRESS: Polymer Science and Engineering, University of Massachusetts, Amherst, Massachusetts 01003	10. PROGRAM ELEMENT, PROJECT, TASK AREA & WORK UNIT NUMBERS
11. CONTROLLING OFFICE NAME AND ADDRESS: Office of Naval Research, 800 North Quincy Street, Arlington, Virginia 22217	12. REPORT DATE: January 5, 1987 13. NUMBER OF PAGES
14. MONITORING AGENCY NAME & ADDRESS (if different from Controlling Office)	15. SECURITY CLASS. (of this report): Unclassified 15a. DECLASSIFICATION/DOWNGRADING SCHEDULE

16. DISTRIBUTION STATEMENT (of this Report)

Approved for public release; distribution unlimited

17. DISTRIBUTION STATEMENT (of the abstract entered in Block 20, if different from Report)

DTIC ELECTE MAR 3 1987 S A

18. SUPPLEMENTARY NOTES

19. KEY WORDS (Continue on reverse side if necessary and identify by block number)

Compressive strength, buckling, high modulus organic fibers, torsional moduli, kink bands, composites

20. ABSTRACT (Continue on reverse side if necessary and identify by block number)

For failure initiated by elastic microbuckling of polymer chains or fibrils, the maximum fiber strength is predicted to be equal to the minimum longitudinal shear modulus of the fiber. An excellent linear correlation between measured strengths and torsion moduli was obtained for four liquid crystalline polymer fibers and high modulus graphite fibers. A correlation shows that measured strengths are 30% of the corresponding torsion moduli, the theoretical strengths, for all these fibers.

DD FORM 1 JAN 73 1473

SECURITY CLASSIFICATION OF THIS PAGE (When Data Entered)

DTIC FILE COPY

87 2 25 019

EXPERIMENTAL VERIFICATION OF A MICROBUCKLING MODEL FOR THE AXIAL COMPRESSIVE FAILURE OF HIGH PERFORMANCE POLYMER FIBERS

By

Steven J. DeTeresa*, Roger S. Porter and Richard J. Farris

Polymer Science and Engineering Department
University of Massachusetts
Amherst, Massachusetts 01003

*Current Address: Composites and Polymers Technology Group
Chemistry and Materials Science Department
Lawrence Livermore National Laboratory
University of California
P.O. Box 808
Livermore, California 94550

ABSTRACT

A previously derived theoretical compressive strength for fibers composed of uniaxially oriented and extended polymer chains was compared with the measured strengths of several high performance fibers. For failure initiated by elastic microbuckling of polymer chains or fibrils, the maximum fiber strength is predicted to be equal to the minimum longitudinal shear modulus of the fiber. An excellent linear correlation between measured strengths and torsion moduli was obtained for four liquid crystalline polymer fibers and high modulus graphite fibers. A correlation shows that measured strengths are 30% of the corresponding torsion moduli, the theoretical strengths, for all these fibers. A high modulus, high strength polyethylene fiber exhibited a compressive strength-torsion modulus ratio that was lower than the value 0.3 obtained for the other fibers examined in this study.

A-1

BACKGROUND

The axial compressive failure of high-performance polymer fibers is manifest as the formation of kink bands[1-6]. Compressive kink bands have been observed to form in many anisotropic materials and structures (see references in [7]). Where the stages of kink band formation were studied, it was concluded that the bands nucleate locally and then propagate through the material[4,8-19].

Independent studies of kink band nucleation in oriented polymers[19], card decks[12] and rubber laminates[13] revealed that local material buckling precedes the collapse into a propagating kink band. Indeed, it is remarkable that the schematic representations of the process of kink band nucleation presented in each diverse study are virtually identical. An example of these representations is shown in Figure 1. These observations suggest that an estimate of the compressive strength of anisotropic materials that form compressive kink bands may be obtained from an elastic microbuckling analysis.

A theoretical compressive strength for high performance polymer fibers has been calculated by the authors using an elastic buckling analysis of a simple model for a collection of uniaxially-oriented and laterally-interacting extended polymer chains[7]. Assuming that the degree of interchain interaction can be characterized by the transverse and shear moduli of the fiber, the following estimate of fiber compressive strength, σ_c, was obtained.

$$\sigma_c = G \tag{1}$$

where G is the longitudinal shear modulus of the fiber.

This simple prediction of compressive strength was obtained, in part, by assuming the fibers to be composed of high molecular weight extended polymer chains. Given this assumption, it can be demonstrated that equation (1) is the critical buckling condition for several simple buckling patterns, some of which are depicted in Figure 2. Comparison of the pattern shown in Figure 2c with those observed in the nucleation region of a kink band (Figure 1) clearly shows the validity of the deformations used in the microbuckling analysis to calculate a theoretical fiber compressive strength. The accuracy of this theoretical value is examined in the present study by comparing measured compressive strengths with longitudinal shear moduli for six high performance fibers.

EXPERIMENTAL

Of the six fibers examined, three are spun from anisotropic solutions of lyotropic liquid crystalline polymers by the dry jet-wet spinning process[20]. These include poly(p-phenylene terephthalamide) (PPTA), poly(p-phenylene benzobisthiazole) (PBT) and poly(2,5-benzoxazole) (ABPBO). All three fibers were tension heat-treated after spinning to improve orientation and thereby increase axial modulus. Kevlar® 49 was the PPTA fiber selected for this study.

A fiber that is melt-spun from an anisotropic melt of a thermotropic liquid crystalline polymer was also examined. This fiber is a nematic thermotropic polyester (NTP) produced by Celanese Co. and it was also subjected to tension heat-treatment after spinning. The chemical structures of all four liquid crystalline polymers are shown in Figure 3.

A high modulus/high strength polyethylene fiber produced by the gel-spinning process[21] was obtained from the Allied Co.

The sixth type of fiber tested is a high modulus graphite fiber (Union Carbide P-75) that is spun from mesophase pitch. This fiber is stretched during the graphitization process to improve orientation and therefore axial modulus[22,23]. Graphite fibers are included in this study of fiber axial compressive strengths because they generally exhibit a structure of axially oriented microfibrillar graphite ribbons having the crystalline graphite basal plane parallel to the long axis of the ribbons[22]. In terms of the model proposed for the extended-chain polymers, the graphite fiber structure can be modelled with laterally-interacting extended graphite sheets that may buckle under compression.

The reasons for selecting a particular graphite fiber are twofold. First, studies of the compressive behavior of graphite fibers show that compressive buckling or kinking only occurs in fibers that have a well-developed and well-oriented graphitic structure[8,24]. These fibers are typically produced by heat-treatment to temperatures near 2800°C and usually exhibit the highest tensile moduli for carbon fibers. Second, the P-75 fiber appears to have a well-developed radial structure; i.e., the graphite basal planes are oriented predominantly parallel to fiber radii (see Figure 4). Therefore, the torsion modulus for such fibers should be nearly equal to the shear modulus for deformation between graphite basal planes. This shear modulus is thus the theoretical estimate of axial compressive strength for graphite fibers that fail due to the microbuckling of extended graphite sheets.

The diameter of fiber samples was measured at several locations along each sample length. The cross-sections of all fibers except PE were circular. Therefore, with the exception of PE, all diameters were measured using a laser diffraction technique[25] that yielded values with a precision of approximately $\pm 2\%$.

The PE fibers had an irregular cross-section that varied significantly along sample lengths. The area and shape of each PE fiber sample was determined, after testing, at several locations along the length by embedding the fiber in a microtome resin followed by cutting transverse sections that were subsequently examined using light microscopy. Micrographs of sections cut from locations ~ 2mm apart along the fiber length were used to determine the cross-sectional area of the fiber by a paper-weighing technique.

Fibers were mounted onto cardboard tabs with epoxy for mechanical tests. Tensile tests were performed on samples with gage lengths ranging from 2-8 cm to allow correction for machine compliance effects[26]. Tensile properties of PE and P-75 graphite fibers were obtained from manufacturers.

The torsion modulus of the fibers was measured using a free torsion pendulum[1]. The equation for calculating the torsion modulus from measurements of underdamped torsional oscillations of a fiber with circular cross-section is given by:

$$G = \frac{8I_d \ell}{\pi \tau^2 r^4} \left[\pi^2 + \frac{(\ln \Delta)^2}{16}\right] \qquad (2)$$

where I_d = polar moment of inertia of disc pendulum

ℓ = sample length

τ = period of oscillation

r = fiber radius

$\ln \Delta$ = logarithmic decrement of amplitude

Torsion pendulum tests were performed at ambient conditions, and damping was noticeable for every fiber tested. However, all values of Δ were found to be >0.5 and therefore, as readily verified from (2), the damping had a negligible effect on the calculated torsion modulus. Hence, the torsion modulus was accurately determined using the approximation:

$$G \simeq \frac{8\pi I_d \ell}{\tau^2 r^4} \qquad (3)$$

Fiber samples 2 cm long were set into torsional oscillation by manually twisting the disc pendulum and then carefully releasing it. This initial twist never exceeded a fiber surface shear strain of ~ >0.5%. The period of oscillation was measured by timing the motion of a mark on the disc pendulum relative to a marked position on a stationary platform placed just beneath the oscillating pendulum.

Two clamp-type aluminum gear blanks were used as disc pendula. The polar moments of inertia of the gear blanks were calculated to be 50.3 and 354 $g\text{-}mm^2$ using dimensions measured with a micrometer (accurate to 1 μm) and weights measured with an analytical balance. The accuracy of these measurements was checked by calculations for the density of aluminum, giving 2.71 and 2.72 g/cc, in excellent agreement with the actual density of 2.699 g/cc. The large pendulum was used for the PE fiber tests and the small one for all other fiber tests.

The fiber axial compressive strengths were calculated from the product of the compressive strain to kink band formation and the axial tensile modulus. This calculation is based on the assumptions that the fibers are linear-elastic up through the compressive strain for initiation of kink bands and that the axial tensile and compressive moduli are identical. The critical compressive strains to kink band formation were measured using a variation of the beam bending technique described previously[1]. In the tests performed here, fibers bonded to the surface of thick transparent elastic beams were compressed by bending the beam in a cantilever mode. This bending configuration sets up a

linear distribution of longitudinal compressive (and tensile) strains along the beam length as shown in Figure 5.

Fibers were examined in the compressed state by holding the beam in the bent configuration during optical microscopic observations. A schematic of a simple rig built for this purpose, which sits on the stage of the optical microscope, is shown in Figure 6.

Fibers were mounted under slight tension (0.5g) onto the surface of 1/2 in x 1/4 in x 6 in Lucite® beams, parallel to the length of the beams, by applying several coats of Krylon® Acrylic Spray. Fibers were tested after allowing the acrylic coating to dry to a hard film. It is emphasized that any shrinkage of the film during drying, which might put residual compressive stresses on the bonded fibers, is prevented by using only a thin acrylic coating on a relatively thick beam.

After a beam with bonded fibers was clamped in the rig as shown in Figure 6, a circular wedge was inserted between the beam and the base plate of the rig to deflect the beam. Bonded, compressed fibers were examined <u>in situ</u> using a transmission light microscope. After insertion of a wedge of known diameter v to a distance L measured from the clamped end of the beam, the distance d from the clamped end to the point along the compressed fiber length where the last kink band was measured. The compressive strain in the fiber at any point x measured from the clamped end is assumed to be equal to the surface strain $\varepsilon(x)$ of the bent beam at the same location. This strain is calculated from:

$$\varepsilon(x) = \frac{3tv}{2L^2}\left(1 - \frac{x}{L}\right) \qquad (4)$$

where t is the thickness of the beam. The critical compressive strain ε_c for kink band formation is defined as the strain at x=d.

The compressive strain distribution in the fiber could be changed either by using a larger diameter wedge or by moving the wedge closer to the clamped end of the beam (i.e., reducing L). In this manner, the remaining undamaged (unkinked) regions of the bonded fiber also could be tested to determine ε_c. Thus, several determinations of ε_c were obtained from one length of fiber. Because the compressive strain for kink band formation was measured, fibers with an irregular cross-section, such as the gel-spun PE, could be tested with the same accuracy as fibers having circular cross-sections.

Equation (4) is derived from linear beam theory, which is based on the assumption of small curvatures for bent beams. Therefore, in all tests performed here, relatively small diameter wedges were held at relatively large distances L so that use of (4) to calculate ε_c would be valid.

The morphology of compressively-kinked fibers was examined using scanning electron microscopy (SEM) and optical microscopy. Kinked fibers were prepared for microscopic observations by using the nylon-6 matrix shrinkage technique for fiber compression described previously[27]. This technique involves the compression of single fibers due to the shrinkage of a surrounding nylon-6 matrix as it is cast from a formic acid solution. Compressed fibers were recovered from the matrix by redissolving the nylon with formic acid.

Tensile tests were performed at strain rates of $\sim 5 \times 10^{-4}$ sec^{-1} using an Instron Universal Testing Machine. A polarizing Zeiss optical microscope was used to examine fibers bonded to bent beams. The surfaces of fibers before and after compression were examined using an ETEC Autoscan SEM.

RESULTS

The range of diameters and the tensile properties measured for each fiber are listed in Table 1. Fibers that are produced in large quantities, namely, PPTA (Kevlar® 49), PBT and P-75 graphite, exhibited relatively uniform diameters along sample lengths. The filament-to-filament variation in diameter for these three fibers was relatively small. The ABPBO and NTP fibers were produced by laboratory-scale spinning processes and were found to exhibit large variations in diameter, both along the length of a filament and between filaments.

Each type of fiber is one variant of a family which exhibits a wide range of tensile properties that depend on spinning and post-heat-treatment conditions. The fibers used in this study were selected because they exhibit some of the best tensile properties attainable for each class of organic material. Although the moduli of these materials cover a range of values, the tensile strengths are all surprisingly similar. The coefficients of variation of tensile strengths ranged from 10-20%. All fibers, except PE, exhibited a linear stress-strain behavior to break. Therefore, a reasonable estimate of strain at break for these fibers is simply the ratio of tensile strength to tensile modulus.

A 2 cm length of PE fiber was tensile-tested to a load below break. This fiber exhibited tensile yield behavior. After testing, the intact fiber was embedded in resin and sectioned to determine the shape and area of the cross-section. The profiles of two transverse sections of this sample taken approximately 1 cm apart are illustrated in Figure 7a. The cross-sectional area was

measured to be 1.1 x 10^3 μm^2. Assuming the fiber "diameter" supplied by the manufacturer was calculated using linear density measurements, this hypothetical diameter corresponds to a cross-sectional area of 1.13 x 10^3 μm^2. Therefore, the areas calculated from micrographs of transverse fiber sections are in excellent agreement with manufacturer's data.

Using a machine compliance value obtained from tensile tests of other fibers under the same test conditions, a tensile modulus of 110 GPa was calculated for the single PE sample tested. Within experimental error, this value is identical to the tensile modulus of 117 GPa quoted by the manufacturer. The limit of proportionality (onset of yielding) occurred at a tensile stress of 170 MPa.

Values of torsion modulus G, critical compressive strain ε_c and calculated axial compressive strengths for each fiber are given in Table 2. Axial compressive strengths of PPTA (Kevlar® 49)[28] and PBT[29] fibers were also obtained by calculating the stress in each fiber at the reported yield or failure load measured in axial compression-testing of unidirectional composites of these fibers. These values are also listed in Table 2.

It was discovered that axial tensile stresses resulted in an apparent increase in the fiber torsion modulus that is given by the equation:

$$G^* = m\sigma + G \qquad (5)$$

where σ is the axial tensile stress, G^* is the apparent torsion modulus, G is the true torsion modulus and m is a constant equal to ~ 0.75. The reasons for, and implications of, this effect will be examined later. For the present, it

is only necessary to consider the increase in measured torsion modulus due to the axial stress generated by the weight of the disc pendulum. Therefore, the corrected values of torsion modulus for each fiber are given in Table 2. For thinner fibers, this correction for pendulum weight amounted to < 10%.

The measured torsion modulus of the P-75 graphite fiber is close to the value of 4.1 GPa reported for the inter-basal plane shear modulus of a dislocation-free graphite crystal[30]. The similarity of these shear moduli is evidence for a radial structure in P-75 graphite fibers.

The largest uncertainty in torsion modulus is for PE fibers, due to their irregular and varying cross-sections. The profiles of cross-sections of 4 test specimens (all 2 cm long) are shown in Figure 7b-e. The torsional rigidities of these specimens were calculated assuming that the cross-sectional profiles could be approximated by an ellipse, rectangle or triangle, whichever most closely fit the particular profile. It should be noted that all 4 specimens were cut from a single filament approximately 12 cm long and examination of Figure 7b-e clearly shows the variation of the PE fiber cross-section along the length of a filament. Although the coefficient of variation of the PE fiber torsion modulus is large, the mean value of 0.7 GPa is in good agreement with the torsion modulus of 0.6 GPa measured for hot-drawn PE monofilaments[31].

In previous studies it was shown that PPTA (Kevlar® 49) fibers form helical kink bands under axial compression[1,27]. SEM and optical micrographs of kink bands in PBT, ABPBO, NTP and PE fibers are shown in Figures 8-11, see Figure 3 for identification of fiber compositions. Except for the PE fiber, no kink

bands were observed in fibers prior to axial compression. Considering the relative thickness of the PE fiber and its low critical strain to kink band formation, the few kinks seen in as-received fiber probably resulted from fiber bending due to handling.

Kink bands initiate in PBT fibers as thin bands oriented at ~ 70° to the fiber axis. The arrow in Figure 8 points to an incipient band. At higher levels of compressive strain, the bands propagate across the fiber and eventually form the thick, bulging perpendicular deformation bands seen in Figures 8c,d. These large bands form periodically along the fiber axis.

The kink bands in compressed ABPBO fibers shown in Figure 9c,d bear some resemblance to the helical kink bands observed in PPTA fibers. Like the PPTA kink bands, the bands in ABPBO fibers are oriented at angles ranging from 50°-60° to the fiber axis. Although the ABPBO compressive kink bands appear to be helical, there is no propagation of any one helical band for any appreciable distance along the fiber length.

In optical micrographs of compressed NTP fibers (Figure 10c), black deformation bands of various thicknesses are observed to be oriented at approximately 55° to the fiber axis. Where only one band crosses the fiber, the deformation closely resembles that being proposed. Where two such bands criss-cross, the fiber exhibits bulging that is similar to the dilatation in deaformation bands in PBT fibers. The surface of compressed NTP fibers exhibits kink bands oriented at several angles to the fiber axis (Figure 10d). There is no obvious regularity to the spacing of these bands along the length of NTP fibers.

Compressed PE fibers exhibit both obliquely oriented kink bands and bands that are oriented at 90° to the fiber axis (Figure 11c,d). In many regions of compressed PE fibers, deformation bands formed at regular intervals along the fiber axis.

The graphite fiber is opaque and thus could not be measured for compressive strength using transmission optical microscopy with the beam bending technique. However, the compressive strengths of similar pitch-based graphite fibers were calculated by other workers who used the elastica test to measure the compressive stress that initiated inelastic behavior[24] and an axial compression test to measure critical compressive strains[8]. The compressive strengths calculated in both studies correspond to the axial compressive stress in the fiber at the onset of localized kinking that appeared on the fiber surface as a deformation band oriented at 90° to the fiber axis. The range of compressive strengths obtained for graphite fiber in these studies is given in Table 2.

The relatively large uncertainties in compressive strengths that were calculated from the product of tensile modulus and critical compressive strains arise from the combined errors in the latter two quantities. However, the range of coefficients of variation for compressive strengths is similar to the range of uncertainty for the tensile strengths.

A comparison of measured compressive strengths with the predicted critical stresses for elastic instabilities, i.e., torsion moduli, is shown in Figure 12. The correlation between these quantities is extremely good for all fibers except PE. The values for PPTA, PBT, ABPBO and NTP fibers can be fitted to a straight

line with correlation coefficient r=0.89. If the compressive strengths of PPTA and PBT fibers calculated from composite data are used for linear correlation, the goodness of fit improves to value r=0.98. The equation that describes this correlation is:

$$\sigma_c = 0.30G \qquad (6)$$

It is also evident from Figure 12 that the relationship between shear modulus and axial compressive strength of graphite fibers can be described by (6).

The microbuckling estimate given by the torsion modulus of PE is much higher than the measured compressive strength. The ratio of measured to predicted strength is only 0.13 for this fiber.

DISCUSSION

The linear relationship between axial compressive strength and torsion modulus measured for the liquid-crystalline polymer and graphite fibers supports the concept of compressive failure due to elastic microbuckling instabilities for these materials. The theoretical compressive strength was assumed to be identical to the longitudinal shear modulus measured from fiber torsion. For liquid-crystalline polymer and graphite fibers, the torsion moduli were essentially 3 times the respective measured compressive strengths. Possible explanations for this disparity include fiber anisotropy, voids, residual stresses and misalignment of polymer chains. The relationship of these factors to the microbuckling analysis for compressive strength has been discussed previously[7]; however some of these factors will be reexamined here in greater detail.

Kevlar® 32-34 and radial graphite fibers are cylindrically orthotropic and hence exhibit two longitudinal shear moduli: G_{rz} and $G_{\theta z}$. Torsion tests of fibers measure $G_{\theta z}$, which is the modulus of shearing between hydrogen-bonded sheets in Kevlar® fibers and between basal planes in radial graphite fibers. Therefore, $G_{\theta z}$ is the lower longitudinal shear modulus for these fibers. The torsion modulus of "onionskin" graphite fibers is due to shearing within the basal planes and is larger than G_{rz}. Thus it is surprising that reported torsion moduli of some graphite fibers[35,36] are much greater than the value of 4.1 GPa determined for shear between dislocation-free graphite basal planes[30]. It must be emphasized that for fibers exhibiting an anisotropy such that $G_{\theta z} > G_{rz}$, the torsion modulus is the wrong estimate for the compressive strength of these materials.

Residual stresses have been shown to exist in graphite[37] and PBT fibers[38]. Indeed, the stresses generated during drying of PBT fibers are believed to be the cause of compressive kinking observed in the dried fibers[38]. Regions of a fiber that are under residual compression will reach critical buckling stresses first. Therefore, premature nucleation of kink bands can occur in such regions.

Although reasonable to assume residual stresses in all the fibers examined, these stresses must have minimal effect on the reduction in axial compressive strength. Significant residual stress would be revealed by the linear correlation analysis of compressive strength versus torsion modulus as a relatively large negative intercept. The data plotted in Figure 12 were fitted to a straight line which passed close to the origin, indicating only a small effect of residual stress on compressive strength. Another way that large residual stresses could exist and affect the compressive strength relationship $\sigma_c = 0.3G$ is if the magnitude of the residual stress in each fiber was directly proportional to the torsion modulus. This is highly unlikely for five different fibers. However, the presence of even small residual axial compressive stresses near the surface of these fibers could explain the initiation of kink bands there.

Small misalignment or curvature of chains and microfibrils should not affect the compressive stress that initiates elastic instabilities. However, under axial compression, these misaligned regions would be subjected to shear stresses that could possibly exceed the shear strength between chains or fibrils. Argon has proposed that axial compressive strengths of fiber

composites are limited by local shear failure along such planes of misalignment[16]. He believes that shear failure initiates material collapse into a kink band. The longitudinal compressive strength of fiber composites that fail in this manner is given by:

$$\sigma_c = \frac{\tau_m}{\phi} \tag{7}$$

where τ_m is the interlaminar shear strength and ϕ is the angle of misalignment measured with respect to load direction.

Fiber will always exhibit a distribution of chain orientation with shear failure occurring in the most poorly aligned regions. Although difficult to measure the largest misalignment angle, it is reasonable to assume, based on Argon's proposal, that fibers with better average orientation should have higher compressive strengths. However, the compressive strengths of PBT[29,39] and Kevlar® [28] fibers are relatively insensitive to the improvements in average axial orientation attained via tension heat-treatment. Thus, it appears unlikely that shear failure initiates compressive kink band formation in these fibers.

The gel-spun PE fiber does not obey the relationship between compressive strength and torsion modulus measured for the rigid rod polymer fibers. The existence of residual entanglements in PE fibers may also severely limit their compressive strength.

As mentioned above for the Kevlar® [49] and graphite fibers, it is necessary to measure the minimum longitudinal shear modulus to predict compressive

strength. If the PE fibers are anisotropic within their cross-section, or if they contain amorphous regions that exhi' it low shear moduli, then it is conceivable that the torsion modulus is not the best estimate of compressive strength.

Although it might be argued that a compressive buckling analysis should not apply to flexible polymer chains, it is emphasized that the analysis reveals that the critical compressive strains for microbuckling is only a function of intermolecular (or interfibrillar) interactions when the chains (or fibrils) are long. Therefore, the buckling stress for a collection of laterally interacting and infinitely flexible extended chains is also equal to the minimum longitudinal shear modulus of such a collection.

SUMMARY

Analysis of a microbuckling model for the axial compressive failure of high performance polymer fibers yields a linear relationship between strength and longitudinal shear modulus. This tight relationship has been verified for liquid crystalline polymer fibers and high modulus graphite fibers, which exhibit axial compressive strengths equal to 30% of their respective torsion moduli.

ACKNOWLEDGEMENT

The authors wish to acknowledge the generous support of this work by the Materials Laboratory of the Air Force, Wright Aeronautical Laboratories, and by the Office of Naval Research. We express thanks to the following companies for supplying the fiber: E.I. DuPont de Nemours & Co. for Kevlar®, Allied-Signal Co. for PE, Celanese Co. for NTP and Union Carbide for P-75 graphite fiber.

REFERENCES

1. S.J. DeTeresa, S.R. Allen, R.J. Farris and R.S. Porter, J. Mater. Sci., 19, 57 (1984).
2. T. Takahashi, M. Miura and K. Sakurai, J. Appl. Polym. Sci., 28, 579 (1983).
3. S.R. Allen, A.G. Filippov, R.J. Farris, E.L. Thomas, C-P. Wong, G.C. Berry and E.C. Chenevey, Macromolecules, 14, 1135 (1981).
4. M.G. Dobb, D.J. Johnson and B.P. Saville, Polymer, 22, 960 (1981).
5. J.M. Greenwood and P.G. Rose, J. Mater. Sci., 9, 1809 (1974).
6. M.M. Schoppee and J. Skelton, Tex. Res. J., 44, 968 (1974).
7. S.J. DeTeresa, R.S. Porter and R.J. Farris, J. Mater. Sci., 20, 1645 (1985).
8. H.M. Hawthorne and E. Teghtsoonian, J. Mater. Sci., 10, 41 (1975).
9. E. Orowan, Nature, 149, 643 (1942).
10. K. Shigematsu, K. Imada and M. Takayanagi, J. Polym. Sci., Polym. Phys. Ed., 13, 73 (1975).
11. M.S. Paterson and L.E. Weiss, Geol. Soc. Amer. Bull., 77, 343 (1966).
12. N.C. Gay and L.E. Weiss, Tectonophysics, 21, 287 (1974).
13. E. Honea and A.M. Johnson, Tectonophysics, 30, 197 (1976).
14. C.W. Weaver and J.G. Williams, J. Mater. Sci., 10, 1323 (1975).
15. C.R. Chaplin, J. Mater. Sci., 12, 347 (1977).
16. A.S. Argon in "Treatise on Materials Science and Technology", edited by H. Herman, Academic Press, NY, 1972, Vol. 1, p. 79.
17. A.G. Evans and W.F. Adler, Acta Metalurgica, 26, 725 (1978).
18. L.E. Weiss, Tectonophysics, 65, 1 (1980).

19. R.E. Robertson, J. Polym. Sci., Part A-2, 7, 1315 (1969).

20. H. Blades, U.S. Patent 3,869,430, assigned to E.I. DuPont de Nemours & Co. (1975).

21. P. Smith and P. Lemstra, J. Mater. Sci., 15, 505 (1980).

22. R.J. Diefendorf and E. Tokarsky, Polym. Eng. Sci., 15, 150 (1975).

23. W.N. Reynolds in "Chemistry and Physics of Carbon", edited by P.L. Walker, Jr., and P.A. Thrower, Marcel Dekker, NY, 1973, Vol. 11, p. 2.

24. W.R. Jones and J.W. Johnson, Carbon, 9, 645 (1971).

25. A.J. Perry, B. Ineichen and B. Eliasson, J. Mater. Sci., Letters, 9, 1376 (1974).

26. ASTM D3379-75e, ASTM, Philadelphia (1975).

27. S.J. DeTeresa, R.S. Porter and R.J. Farris, Polym. Comp., 2, 57 (1982).

28. R.E. Wilfong and J. Zimmerman, J. Appl. Polym. Sci., Appl. Polym. Symp., 31, 1 (1977).

29. J.F. Mammone and W.C. Uy, Air Force Technical Report, AFML-TR-82-4154 (1984).

30. E.J. Seldin and C.W. Nezbeda, J. Appl. Phys., 41, 3389 (1970).

31. D.W. Hadley, P.R. Pinnock and I.M. Ward, J. Mater. Sci., 4, 152 (1969).

32. M.G. Dobb, D.J. Johnson and B.P. Saville, J. Polym. Sci., Polym. Phys. Ed., 15, 2201 (1977).

33. R. Hagege, M. Jarrin and M.J. Sotton, J. Microsc. O., 115, 65 (1979).

34. S.B. Warner, Macromolecules, 16, 1546 (1983).

35. R. Bacon in "Chemistry and Physics of Carbon", edited by P.L. Walker, Jr., and P.A. Thrower, Marcel Dekker, NY, 1973, Vol. 9, p. 80.

36. J-B. Donnet and R.C. Bansal in "Carbon Fibers", Marcel Dekker, NY, 1984, p. 171.

37. K. Chen, C.W. LeMaistre, J.H. Wang and R.J. Diefendorf, 182nd Nat. Conf., ACS, Poly 137, New York, August (1981).

38. S.R. Allen, A.G. Filippov, R.J. Farris and E.L. Thomas, J. Appl. Polym. Sci., 26, 291 (1981).

39. S.R. Allen in "Mechanical and Morphological Correlations in Poly(p-Phenylene Benzobisthiazole) Fibers", Ph.D. Thesis, University of Massachusetts, Amherst, 1983.

Table 1. Tensile Properties of Fibers

Fiber	Diameter Range (μm)	Modulus (GPa)	Strength Break (GPa)
PPTA	11.4-12.8	123 ±5.7	3.2 ±0.16
PBT	12.4-13.5	265 ±15	2.6 ±0.20
ABPBO	13.2-18.1	120 ±10	3.0 ±0.55
NTP	18.7-26.1	77 ±2.9	3.2 ±0.64
PE	(38)*	117*	2.6*
P-75	9.7-10.0	500*	2.0*

*Manufacturer's data

± values are standard deviations.

Table 2. Torsion Moduli and Compressive Strengths of Fibers

Fiber	Torsion Modulus (GPa)[a]	Critical Compressive Strains (%)[b]	Calculated Compressive Strengths (GPa)	Composite Compressive Strength (GPa)[c]
PPTA	1.5 ±0.20	0.50 ±0.03	0.62 ±0.06	0.45[e]
PBT	1.2 ±0.14	0.10 ±0.02	0.27 ±0.08	0.31[f]
ABPBO	0.62 ±0.07	0.18 ±0.03	0.21 ±0.06	
NTP	0.45 ±0.04	0.15 ±0.01	0.12 ±0.01	
PE	0.7 ±0.22	0.08 ±0.015	0.09 ±0.02	
P-75	5.6	-	1.3-2.0[d]	

[a]Corrected for pendulum weight.

[b]Corrected for tensile prestrain applied during mounting to beam.

[c]Calculated from σ_c/V_f, where σ_c = fiber composite 0° compressive strength, V_f = fiber volume fraction of composite.

[d]References 8, 24.

[e]Reference 28.

[f]Reference 29.

± Standard deviations.

FIGURE CAPTIONS

Figure 1: Representation of kink band formation.

Figure 2: Possible microbuckling deformations for a collection of long, extended polymer chains. (Each line represents a single chain.)

Figure 3: Chemical structures of liquid crystalline polymer fibers.

Figure 4: SEM micrograph of the tensile fracture surface of P-75 graphite fiber.

Figure 5: Longitudinally distributed axial normal strains in an elastic beam loaded in cantilever bending.

Figure 6: Schematic of the apparatus used to determine critical compressive strain for kink band formation in single fibers.

Figure 7: Tracings of optical micrographs of transverse sections of PE fibers. (a) Filament 1: tensile test samples. (b-e) Filament 2: torsion test samples.

Figure 8: PBT fiber. Before compression: (a) optical micrograph, (b) SEM micrograph. After compression: (c) optical micrograph, (d) SEM micrograph.

Figure 9: ABPO fiber. Before compression: (a) optical micrograph, (b) SEM micrograph. After compression: (c) optical micrograph, (d) SEM micrograph.

Figure 10: NTP fiber. Before compression: (a) optical micrograph, (b) SEM micrograph. After compression: (c) optical micrograph, (d) SEM micrograph.

Figure 11: PE fiber. Before compression: (a) optical micrograph, (b) SEM micrograph. After compression: (c) optical micrograph, (d) SEM micrograph.

Figure 12: Correlation between measured axial compressive strengths and torsion moduli for high performance organic fibers.

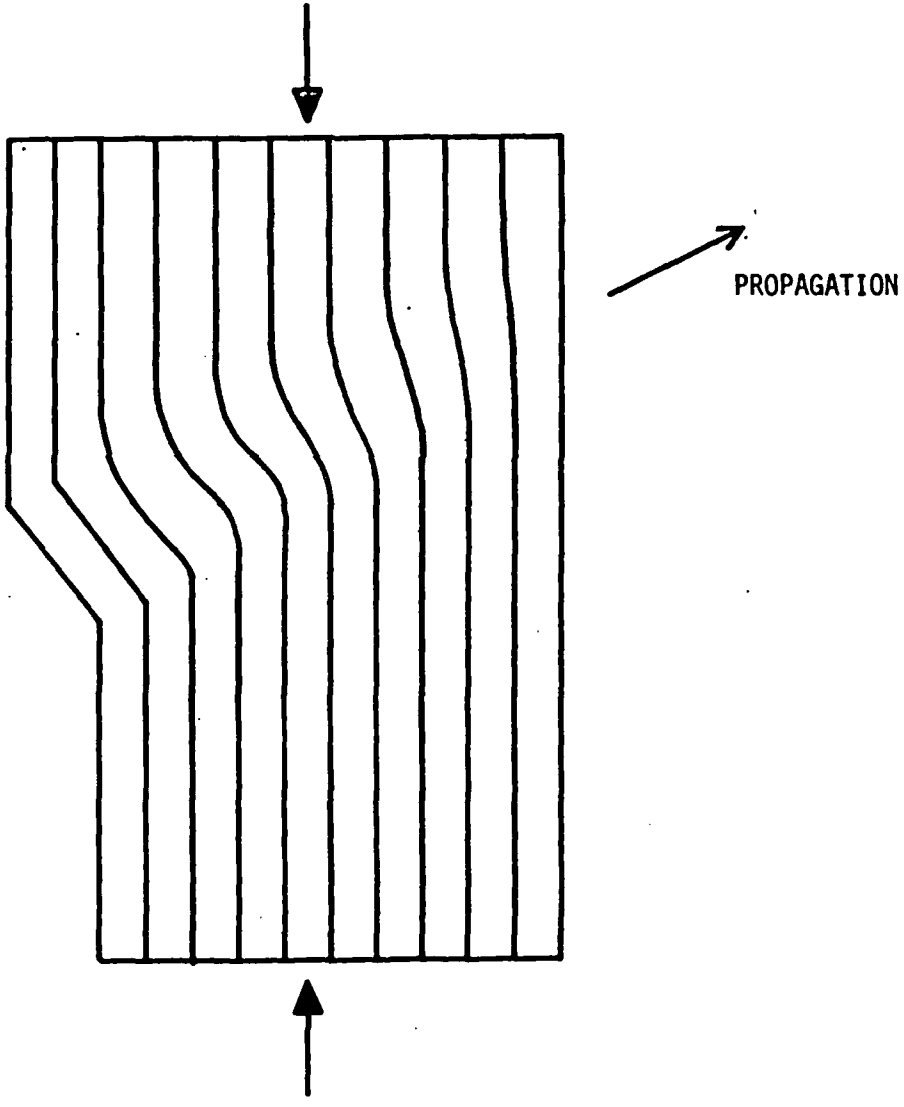

Figure 1.

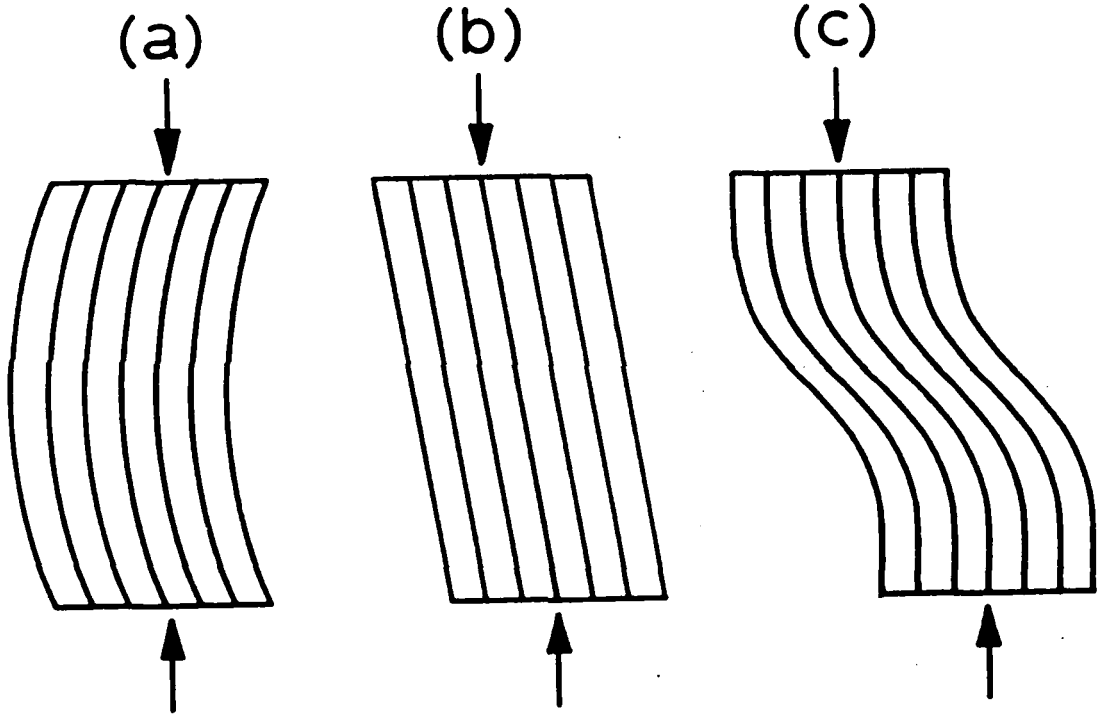

Figure 2.

PPTA

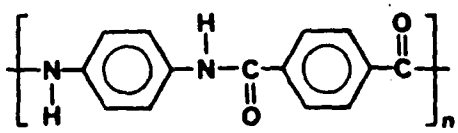

PBT

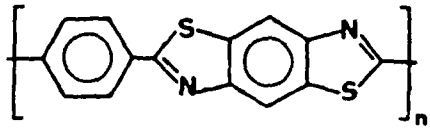

ABPBO

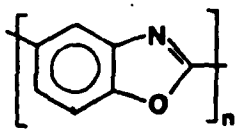

NTP

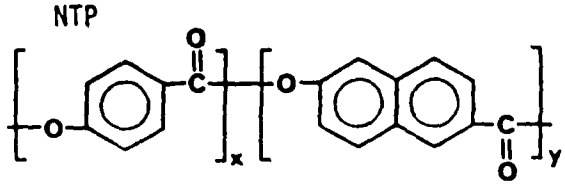

Figure 3

Figure 4

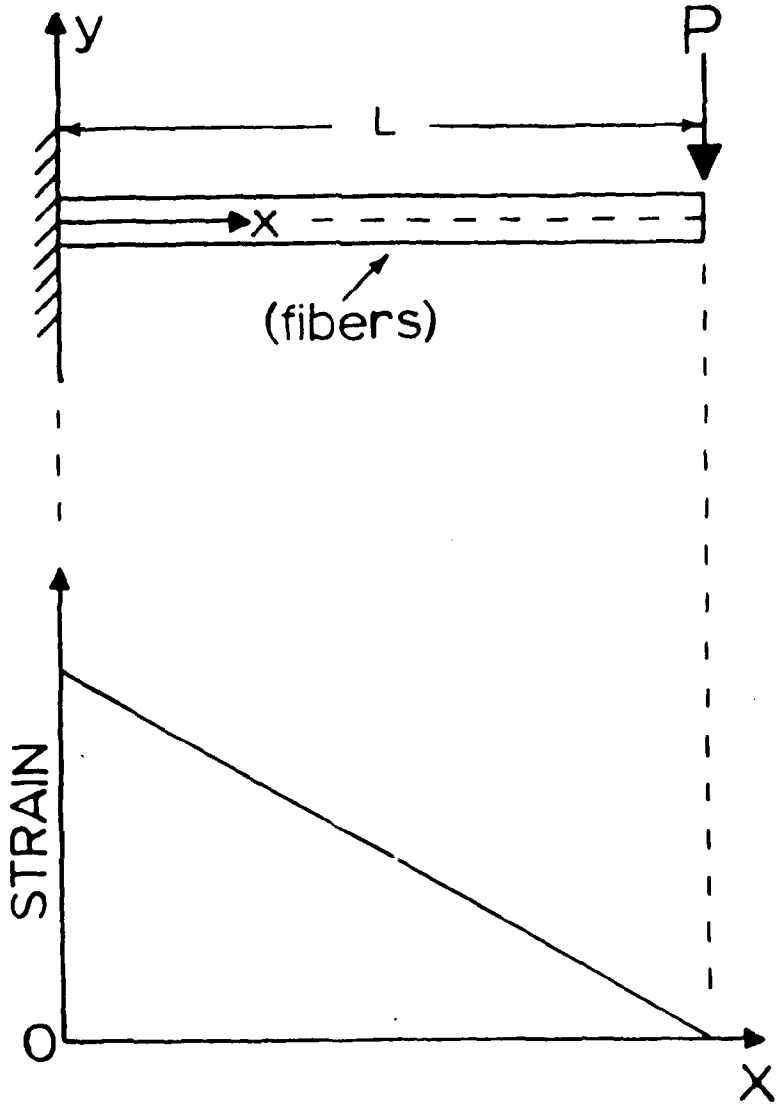

Figure 5

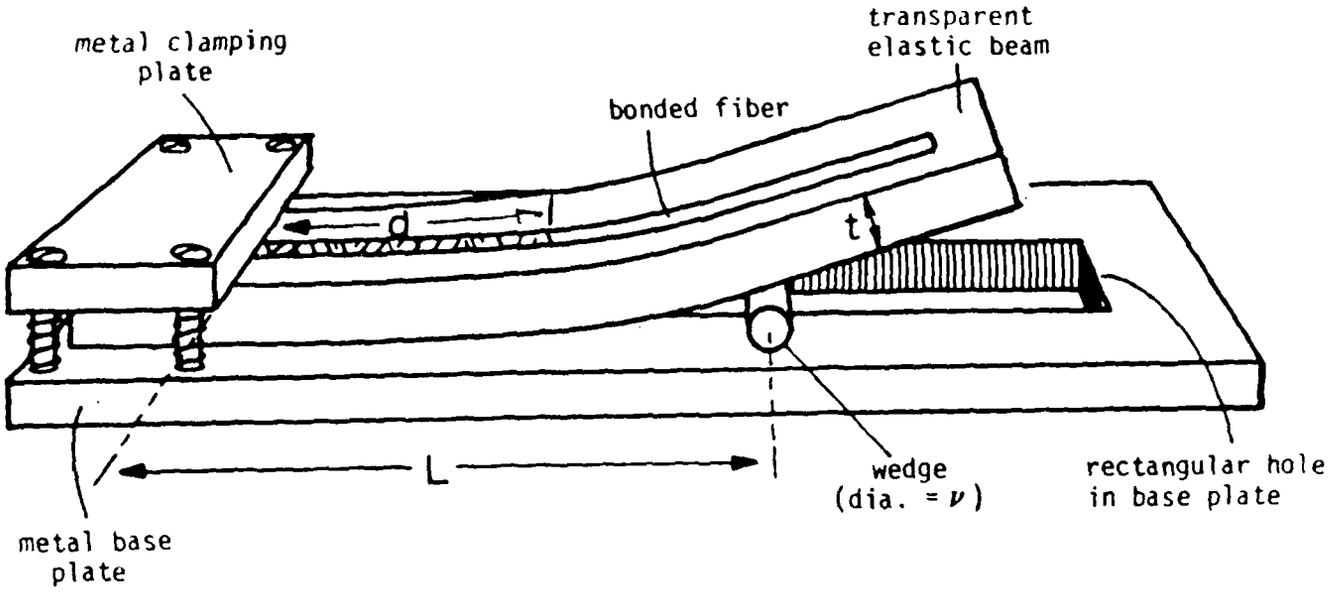
metal clamping plate
transparent elastic beam
bonded fiber
d
t
L
wedge (dia. = ν)
rectangular hole in base plate
metal base plate

Figure 6

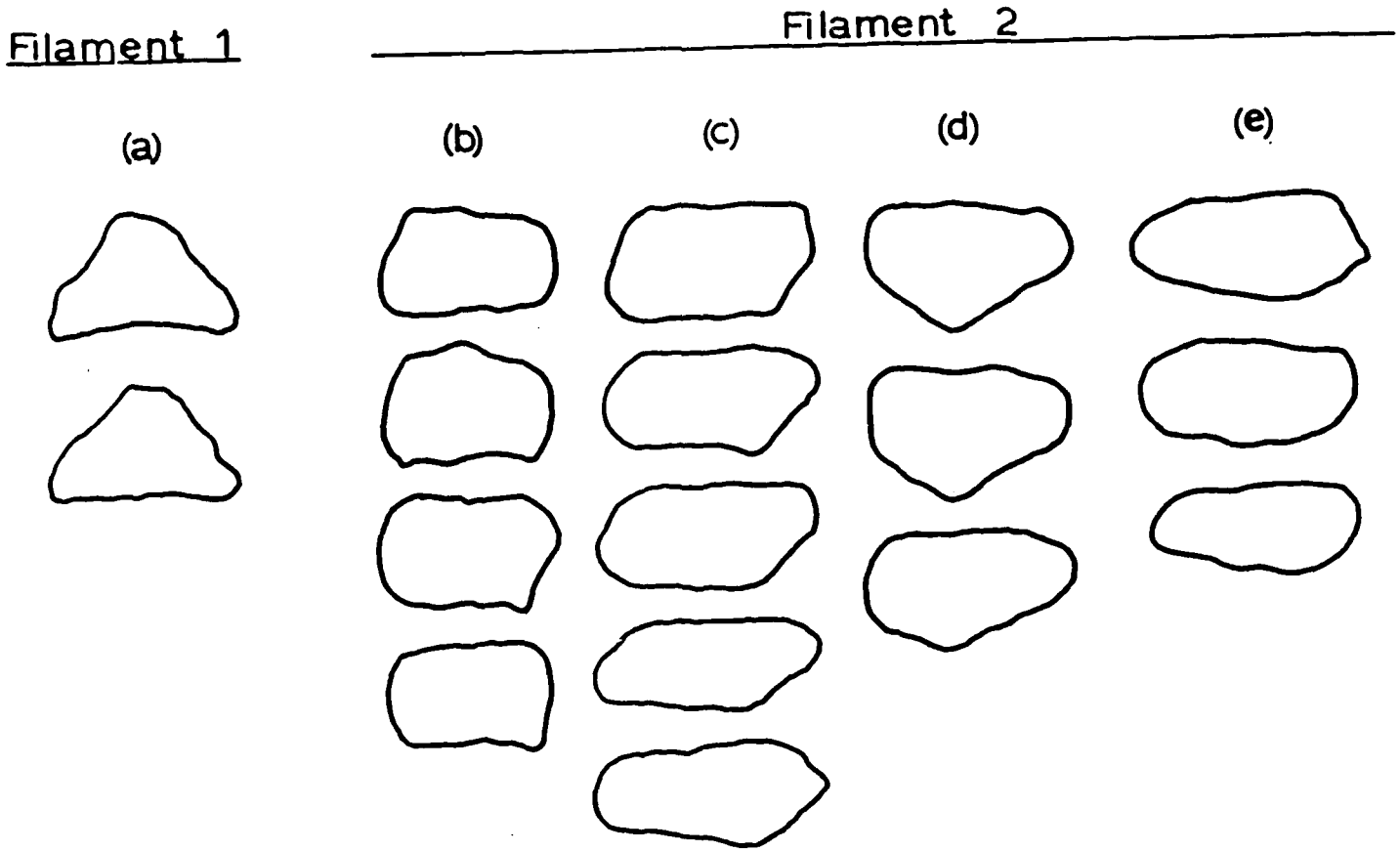

Figure 7

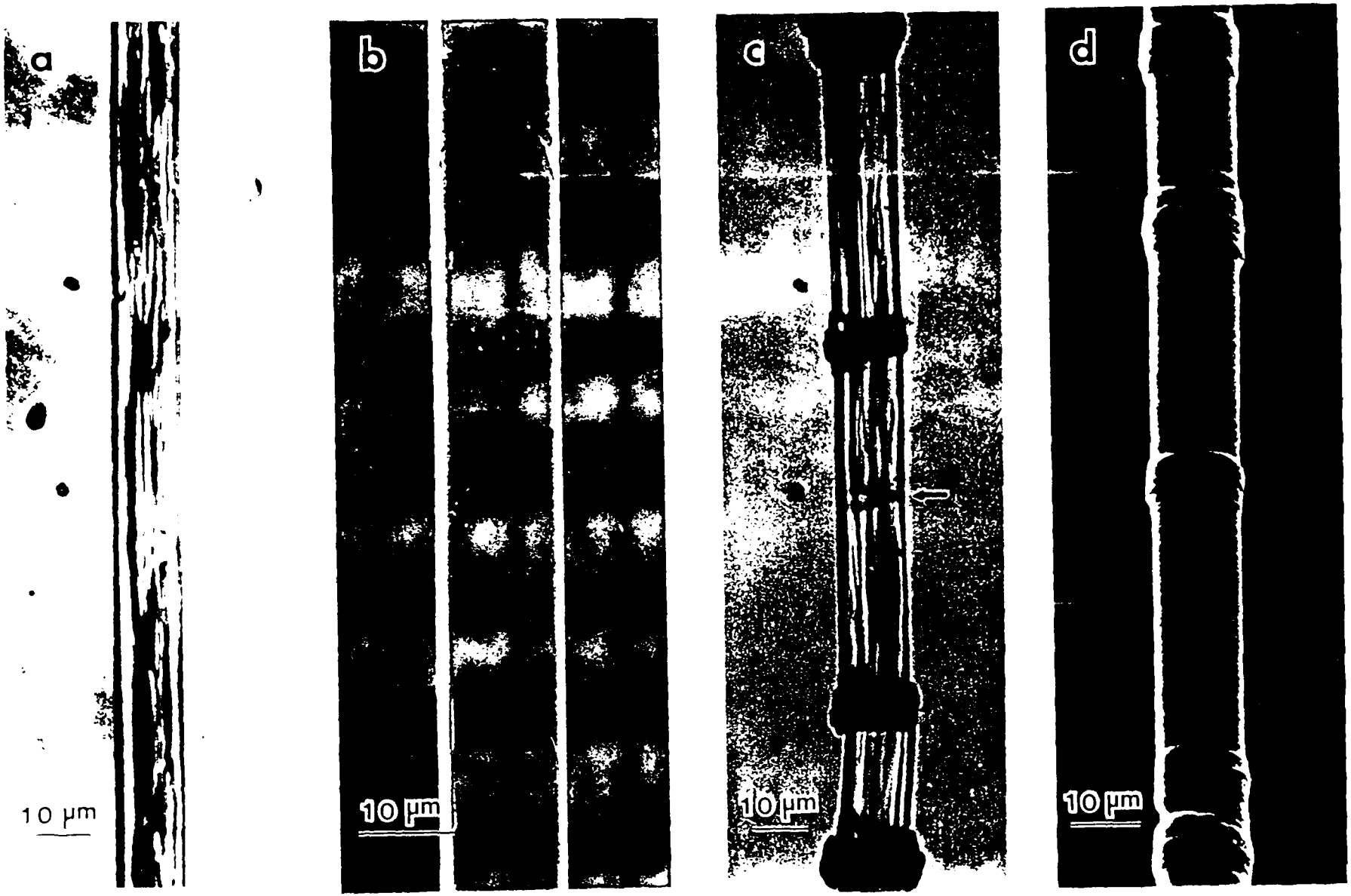

Figure 8.

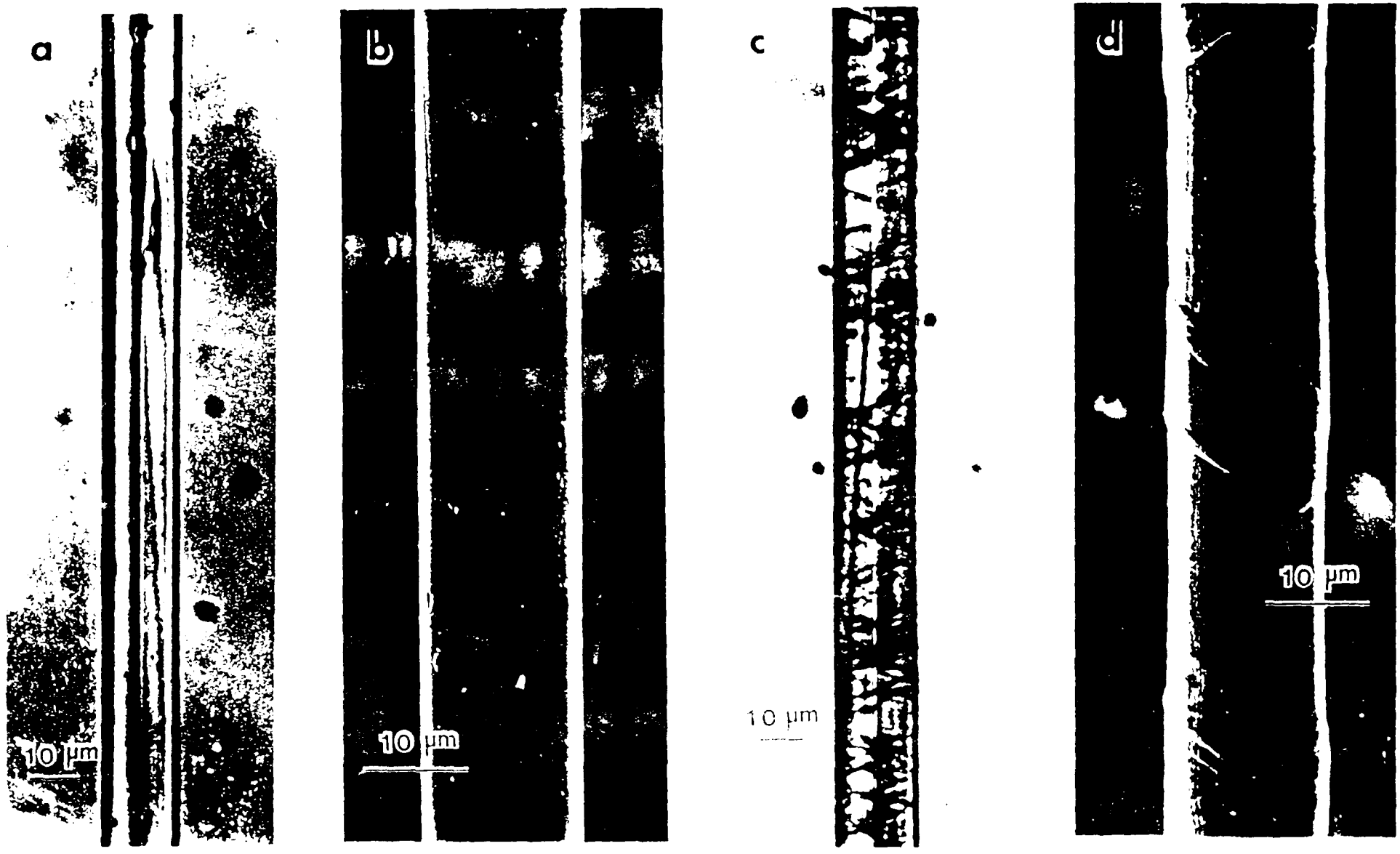

Figure 9.

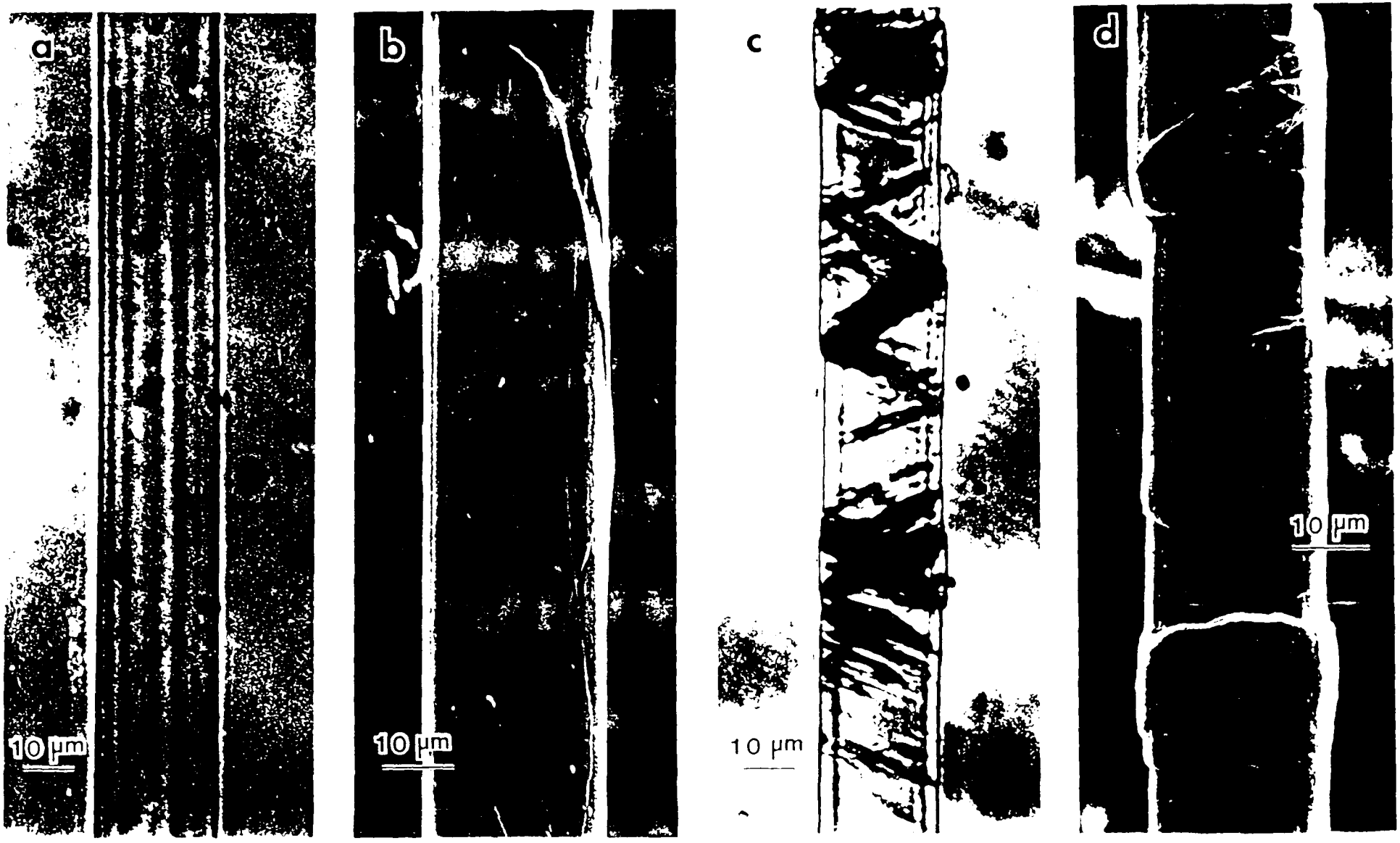

Figure 10

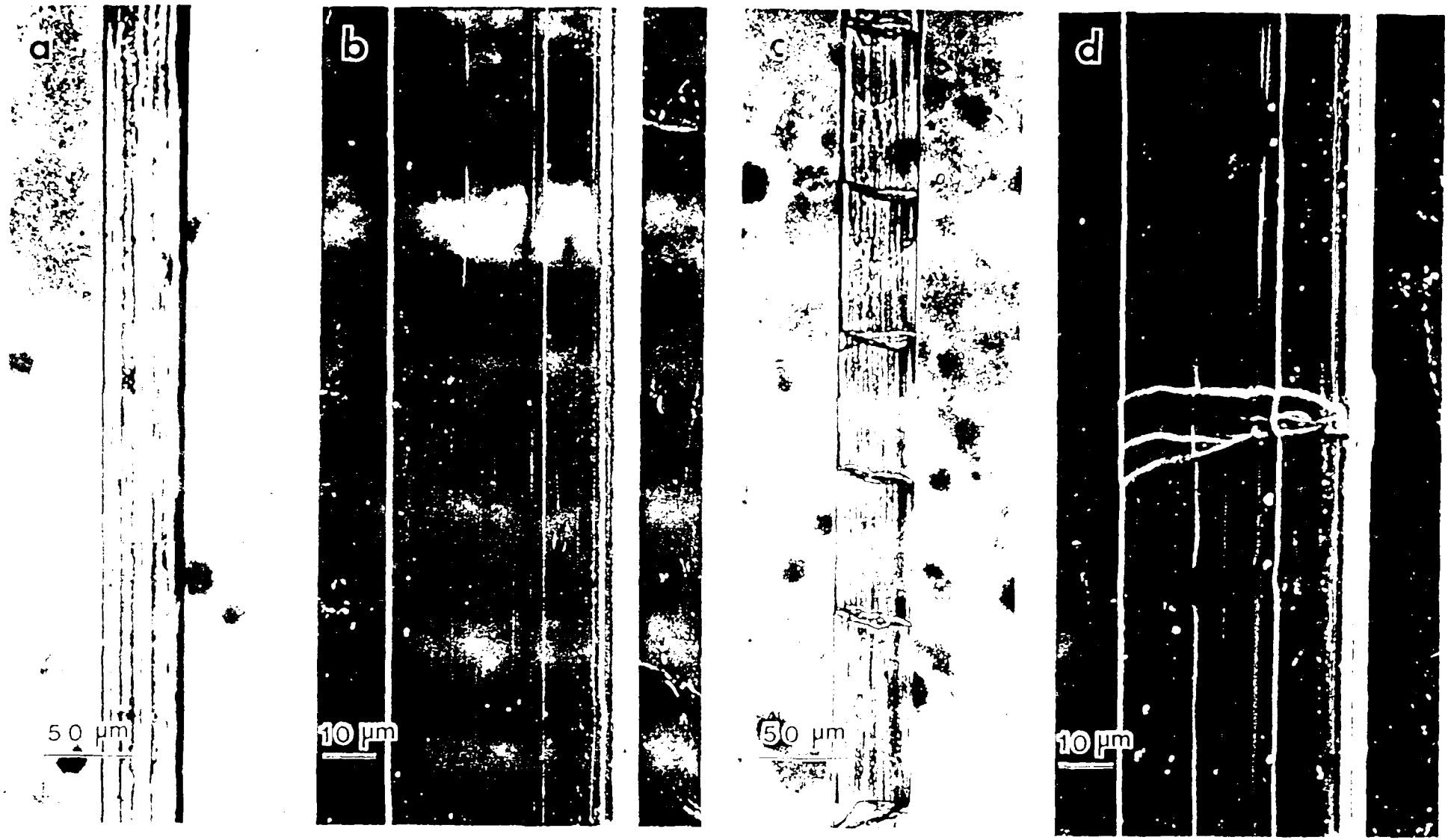

Figure 11

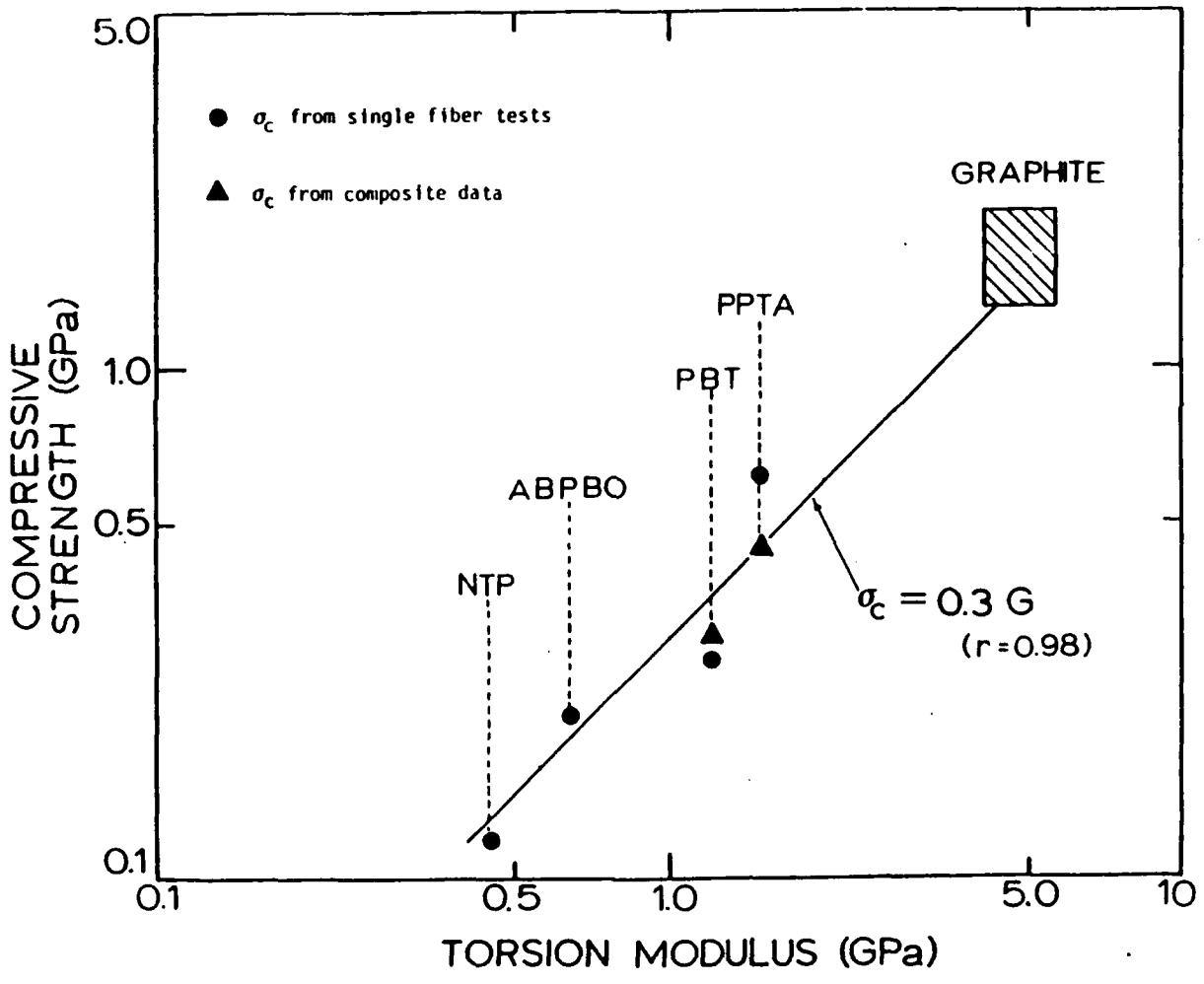
5.0
1.0
0.5
0.1
0.1
0.5
1.0
5.0
10
COMPRESSIVE STRENGTH (GPa)
TORSION MODULUS (GPa)
σ_c from single fiber tests
σ_c from composite data
GRAPHITE
PPTA
PBT
ABPBO
NTP
$\sigma_c = 0.3\ G$
(r = 0.98)

Figure 12.

END

4-88-87

DTIC